2137-33

Joint ICTP-IAEA Advanced Workshop on Multi-Scale Modelling for Characterization and Basic Understanding of Radiation Damage Mechanisms in Materials

12 - 23 April 2010

Radiation damage summary

M. Victoria

*Nuclear Fusion Institute, Universidad Politecnica de Madrid
Spain*

The experimental validation of radiation damage modeling: an "historical" perspective

III. Fe, steels and other bcc metals

Max Victoria

Visiting Professor, UPM

Introduction

- The magnetic behavior of Fe has in general not been taken into account in radiation damage calculations performed up to the late 90's

- As a result, these calculations ignored early experimental results that indicated that the minimun energy configuration of interstitial defects was different from that resultant from the calculations
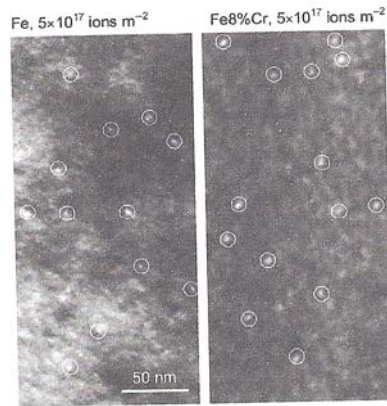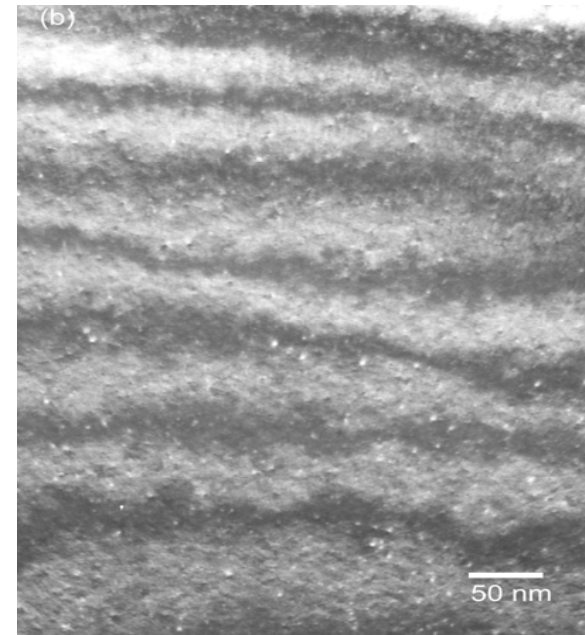
Defect microstructures in Fe

Philosophical Magazine   2857

Fe, 5×10^{17} ions m^{-2} Fe8%Cr, 5×10^{17} ions m^{-2}

50 nm

Figure 1. Small dislocation loops in (110) UHP Fe and (113) UHP Fe–8% Cr irradiated with 150 keV Fe$^+$ ions to a dose of 5×10^{17} m^{-2} ions at RT. The micrographs were taken under weak beam conditions, $(g, \sim3g)$ using the reflection $g = 1\bar{1}0$.

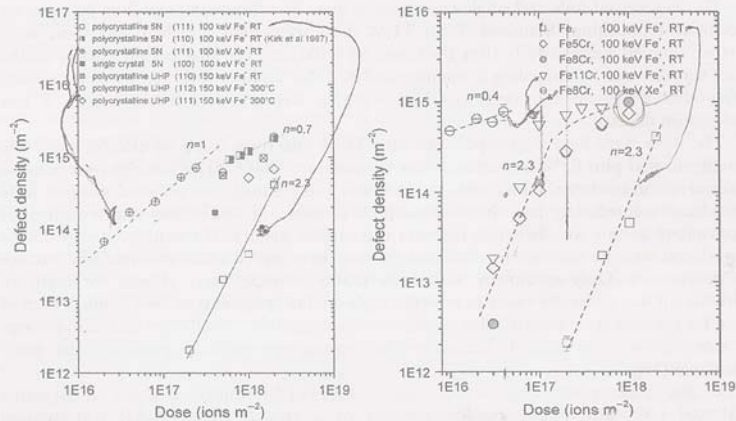2858   Z. Yao et al.

Figure 3. (a) Defect areal densities versus dose for pure Fe. For polycrystalline specimens the approximate orientations of the grains used in the experiments are indicated; the true grain orientations were usually several degrees off the pole. Some representative error bars are shown. Values n of the slopes are shown. (b) Loop areal densities as a function of dose in Fe–Cr alloys irradiated at RT with 100 keV ions in foils oriented close to (111).
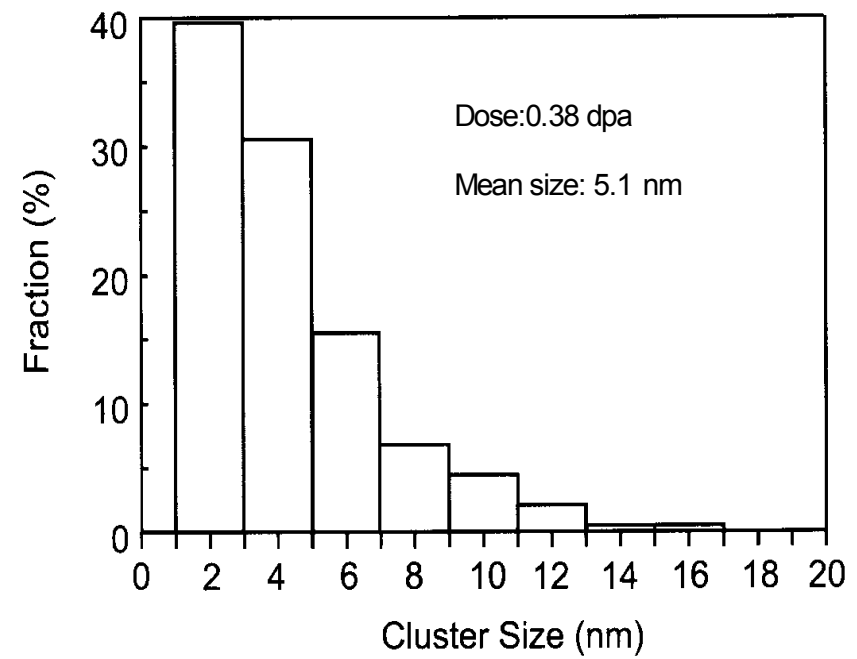
Yao et al (2008)

Luppo et al (2000)

Cluster size distribution in irradiated Fe

Dose: 0.38 dpa
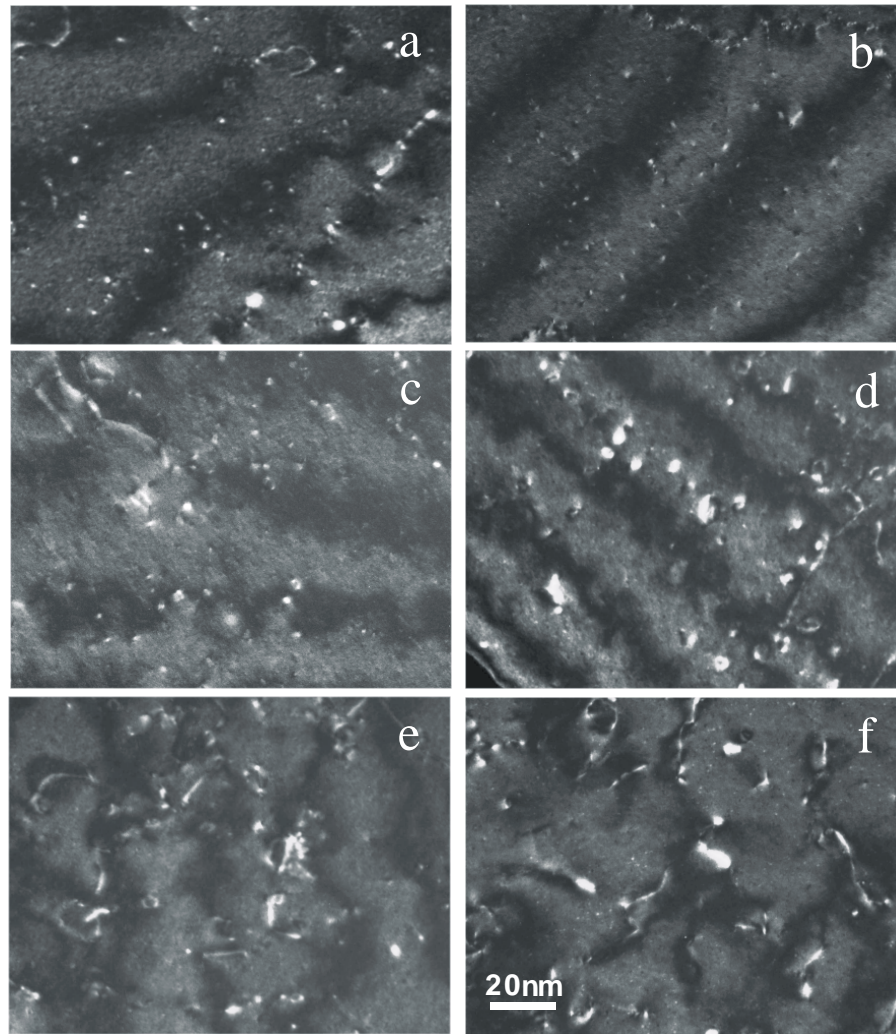
Mean size: 5.1 nm
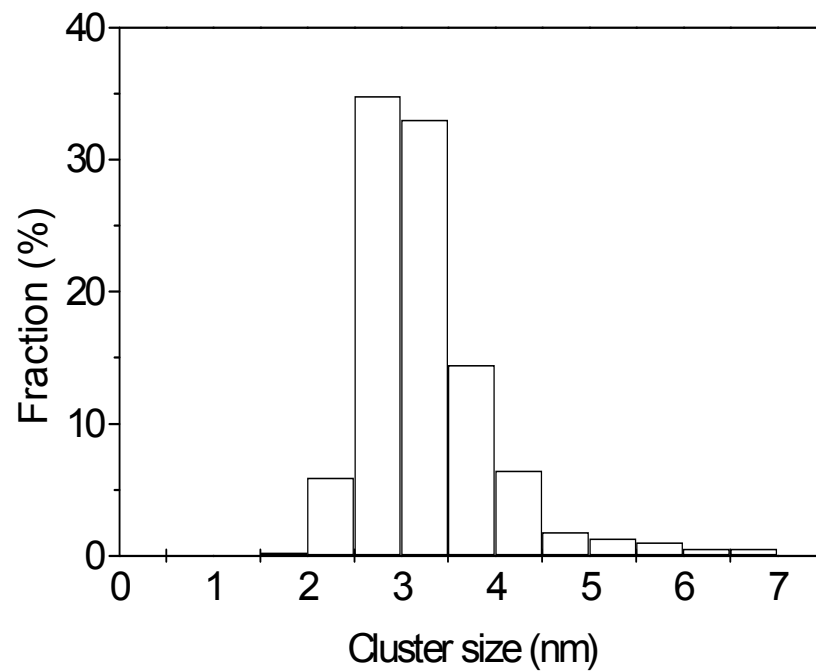
p⁺ (0.33 dpa)

n (0.38 dpa)

Postirradiation defect microstructure

F82H steel irradiated in SINQ

(a) 10   dpa; 140^0 C

(b) 10.2 dpa: 175^0 C

(c) 10.2 dpa; 210^0 C

(d) 10.3 dpa; 255^0 C

(e)   9.9 dpa; 295^0 C

Damage accumulation in α-Fe

- Prevailing vue (Bacon and Osetsky, 2003) based on modeling using empirical potentials:

a) SIA´s: <111> and <110> configurations have comparable energies

b) The same potentials predict that clusters of two or more SIAs form a set of parallel dumbbells moving rapidly in the <111> direction with activation energies ~0.01 eV.

c) But measured migration values are much higher: 0.3 eV for SIAs and 0.42 eV for small clusters

Damage accumulation in α-Fe

In fact experimental results indicate that

- <110> dumbbell configuration established from a number of experimental methods (Schultz (1982), Takaki (1983), Ehrhart (1986)) with a mobility of Ei_m=0.27 eV.

- Very early neutron irradiation experiments performed in not very pure Fe at He temperatures: no annealing peak of RR observed at low T

- Post- morten TEM observations show only <111> and <100> loops

Interstitial configurations in bcc
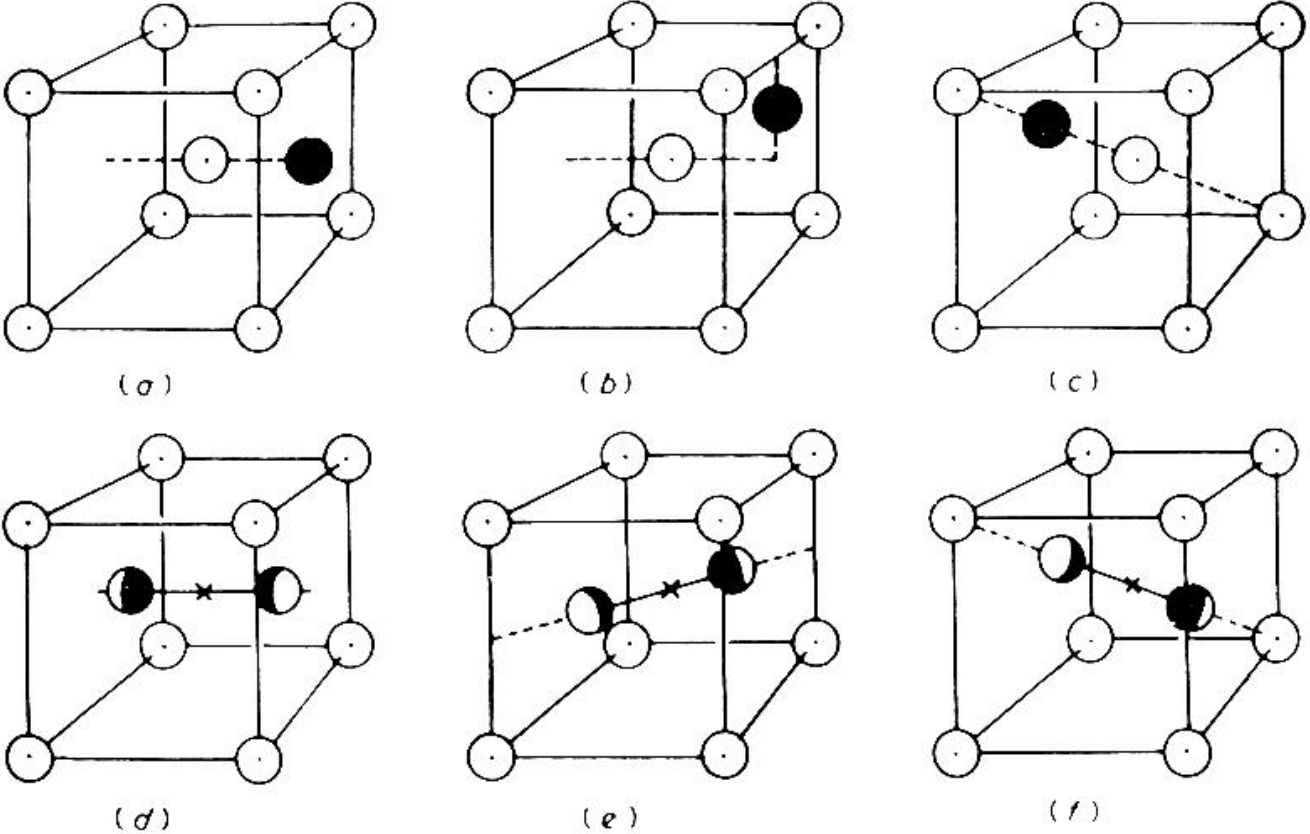
Self-interstitial configurations in a bcc lattice (Johnson 1973): (a) octahedral, (b) tetra-hedral, (c) crowdion, (d) (100)-split (dumbbell), (e) (110)-split, (f) (111)-split.

Magnetism is important in α-Fe and controls its singular behavior amongst bcc metals

Basic parameters of bcc transition metals and formations energies of defects, calculated using DFT. Italics: experimental values.

From D. Nguyen-Manh *et al* (2006)

	V	Nb	Ta	Cr	Mo	W	Fe
a (Å)	3.04	3.32	3.31	2.85	3.17	3.18	2.88
	3.03	*3.30*	*3.30*	*2.88*	*3.15*	*3.16*	*2.87*
B (Mbar)	1.71	1.73	1.99	1.92	2.68	3.05	1.80
	1.62	*1.70*	*2.00*	*1.90*	*2.72*	*3.23*	*1.68*
H^v (eV)	2.51	2.99	3.14	2.64	2.96	3.56	2.07
	2.1–2.2	*2.6–3.1*	*2.8–3.1*	*2.0–2.4*	*2.6–3.2*	*3.5–4.1*	*1.8 – 2.2*
H_m^v (eV)	0.62	0.91	1.48	0.91	1.28	1.78	0.67
	0.5-1.2	*0.6-1.0*	*0.7-1.9*	*0.95*	*1.3-1.6*	*1.7–2.0*	*0.55*
⟨111⟩	3.367	5.253	5.832	5.685	7.417	9.548	4.45
dumbbell	*3.14*	*4.795*	*7.157*		*7.34*	*8.919*	
⟨111⟩	3.371	5.254	5.836	5.660	7.419	9.551	4.45
crowdion	*3.15*	*4.857*	*7.158*		*7.34*	*8.893*	
⟨110⟩	3.652	5.597	6.382	5.674	7.581	9.844	3.75
	3.48	*4.482*	*6.847*		*7.51*	*9.641*	
tetrahedral	3.835	5.758	6.771	6.189	8.401	11.05	4.26
	3.69				*8.20*		
⟨100⟩	3.918	5.949	7.003	6.643	9.004	11.49	4.75
	3.57	*4.821*	*8.068*		*8.77*	*9.815*	
octahedral	3.964	6.060	7.095	6.723	9.067	11.68	4.94
	3.62				*8.86*		

Disagreement resolved by *ab initio* calculations

The disagreement was solved by DFT calculations (Fu, Willaime and Ordejon, Phys Rev Let 2004) in which the energies of the different interstitial configurations were obtained for Fe, showing that the <110> dumbbell configuration has an energy lower than the<111> by 0.7 eV.

This is a consequence of magnetism in Fe. For all other bcc metals in the Periodic Table, it is the <111> dumbbell configuration which has the lower energy

The effects of magnetism in Fe and its alloys has led to the need to develop magnetic potentials (Dudarev and Derlet (2005)) or semi-empirical potentials where the effects of magnetism ([110] dumbbell as minimum energy configuration) are included.

Practically all the microscopic processes associate with the irradiated microstructure evolution are thermally activated. The rate at which a given event takes place is given by the Arrhenius law

$$\nu = \nu_0 \exp\left(-Q / k_B T\right)$$

Because it is in an exponential Q needs to be defined with good precision. Present day DFT calculations can reach the accuracies needed, of the order of 0.1 eV. The migration of the SIA in Fe takes place by a translation-rotation mechanism with a migration energy of 0.34 eV
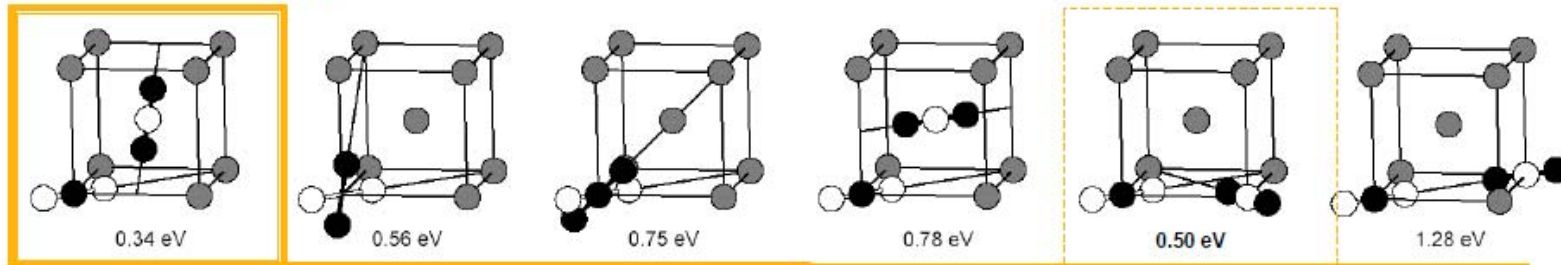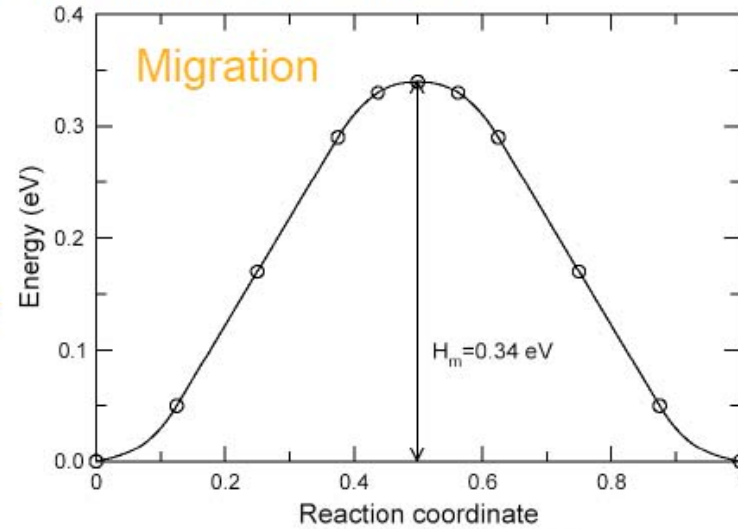
DFT modelling of SIA defects

D. Nguyen Manh, S. L. Dudarev and A. Horsfield (2004)
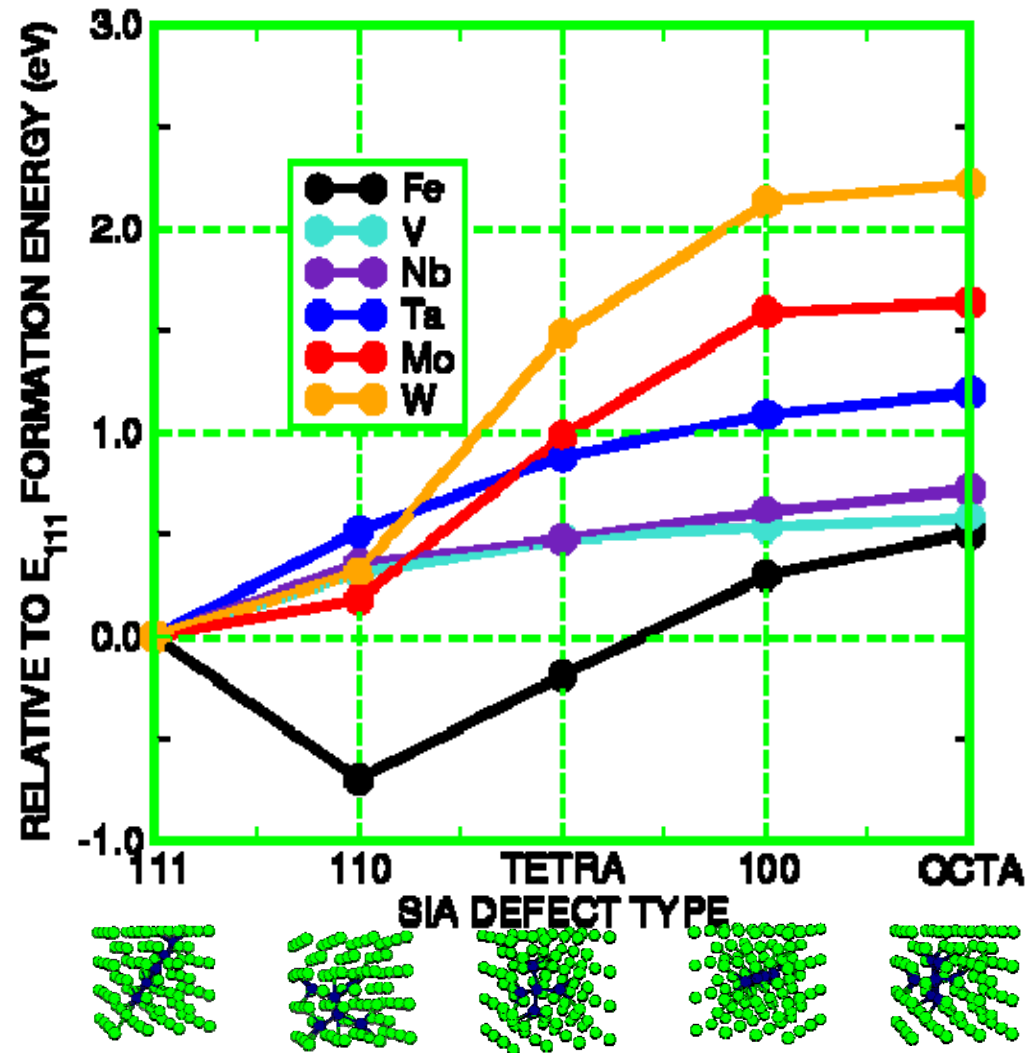
Self-interstitials in BBC Fe

Chu Chun Fu & F. Willaime 2003-2004

Migration mechanisms
of <110> dumbbells

and diffusion path

Migration

H_m=0.34 eV

0.34 eV   0.56 eV   0.75 eV   0.78 eV   0.50 eV   1.28 eV

Translation / rotation 1st neighbour jump → 3D Migration
Excellent agreement with experiment : H_m=0.3 eV
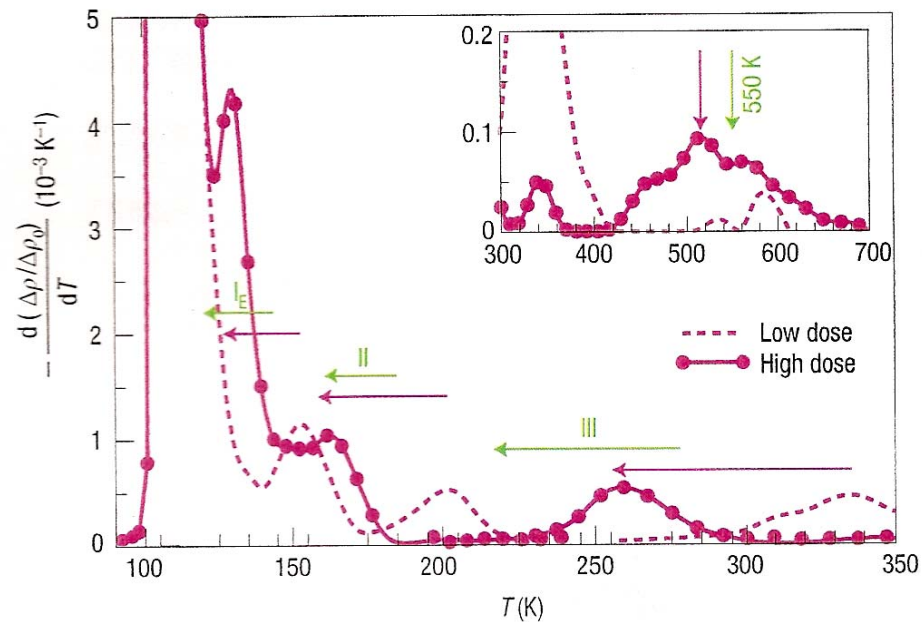
Figure 5 Effect of irradiation dose. Derivative with respect to temperature of the resistivity recovery in the case of high irradiation dose (magenta solid line). The low-dose simulation is from Fig. 4 (dashed line). The beginning and the end of the horizontal arrows indicate the stage temperatures at low and high irradiation doses (2×10^{-6} and 200×10^{-6} dpa respectively): green arrows for experiments and magenta arrows for the simulation. Stage (IV) is shown in the inset.
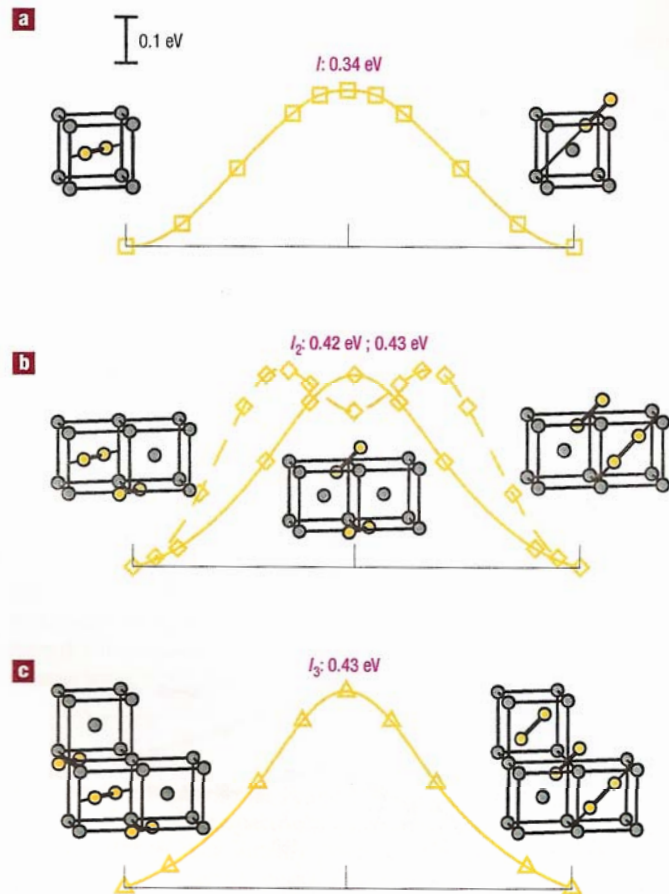
Figure 2 Migration of interstitial-type defects. Energy variation along the most favourable migration pathways for I, I_2 and I_3, determined by *ab initio* calculations. The corresponding migration energies and schematic representations of the migration mechanisms starting from the defect ground-states are shown: the orange and grey spheres indicate self-interstitial and lattice atoms respectively. The energy scale is the same for all graphs.
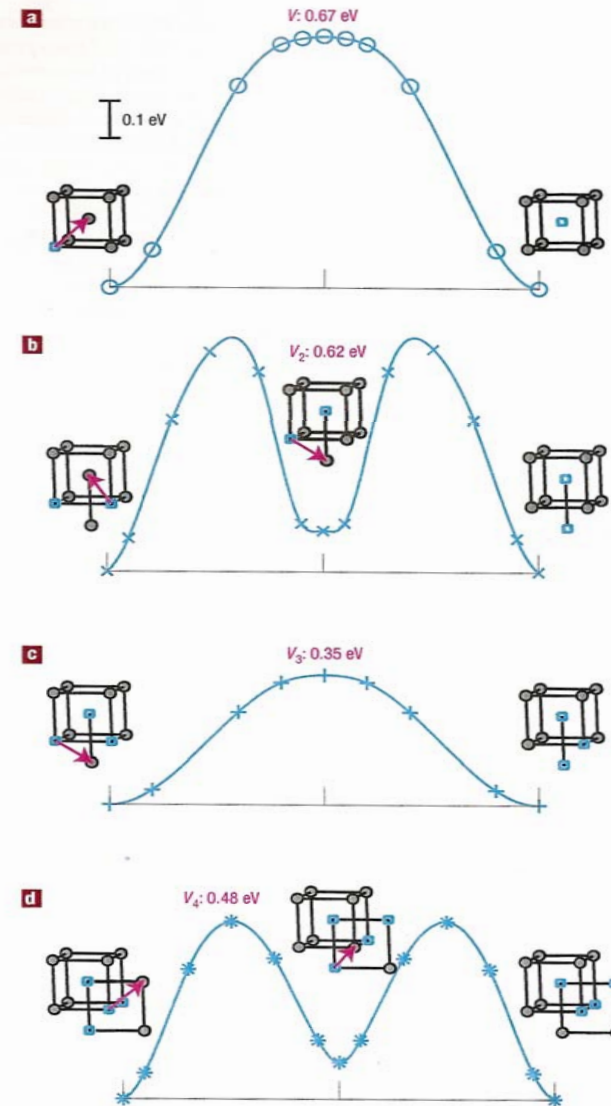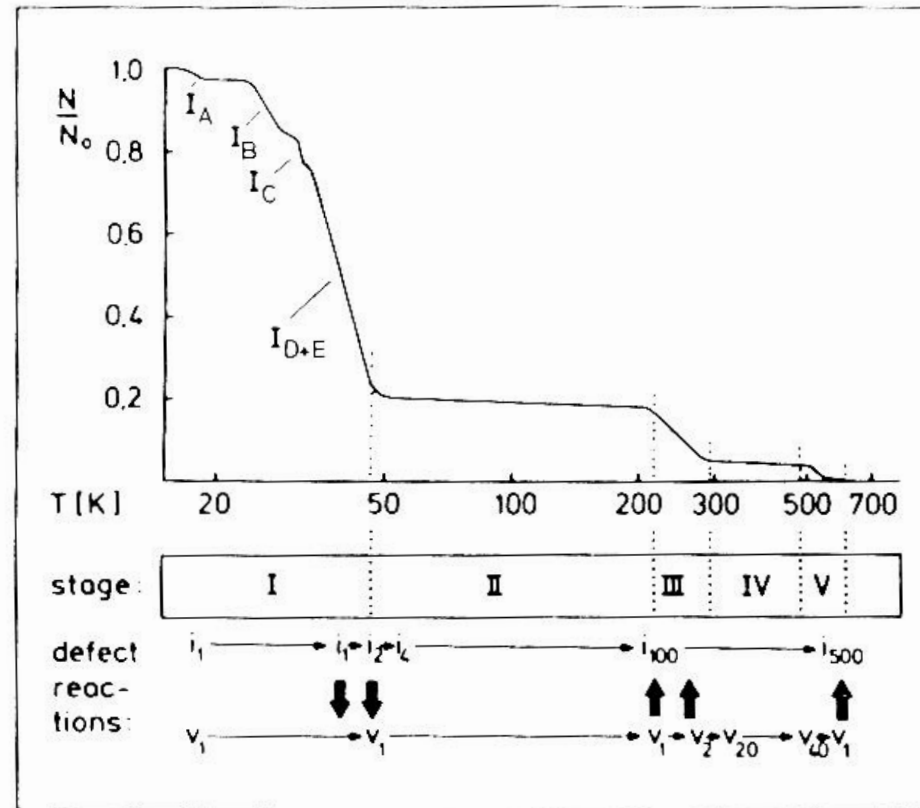
Figure 3 Migration of vacancy-type defects. Energy variation along the most favourable migration pathways for V, V_2, V_3 and V_4. The vacant sites are represented by blue cubes, and their migration jumps by magenta arrows. The energy scales are the same as in Fig. 2 for comparison.

Annealing of electrical resistivity

Annealing stages and defect reactions in pure copper after electron irradiation; i_1, a v_1 denote single interstitials and vacancies, respectively. i_2 and v_2 di-interstitials and divacanci (Schilling et al. 1975.)

The time evolution of the microstructure
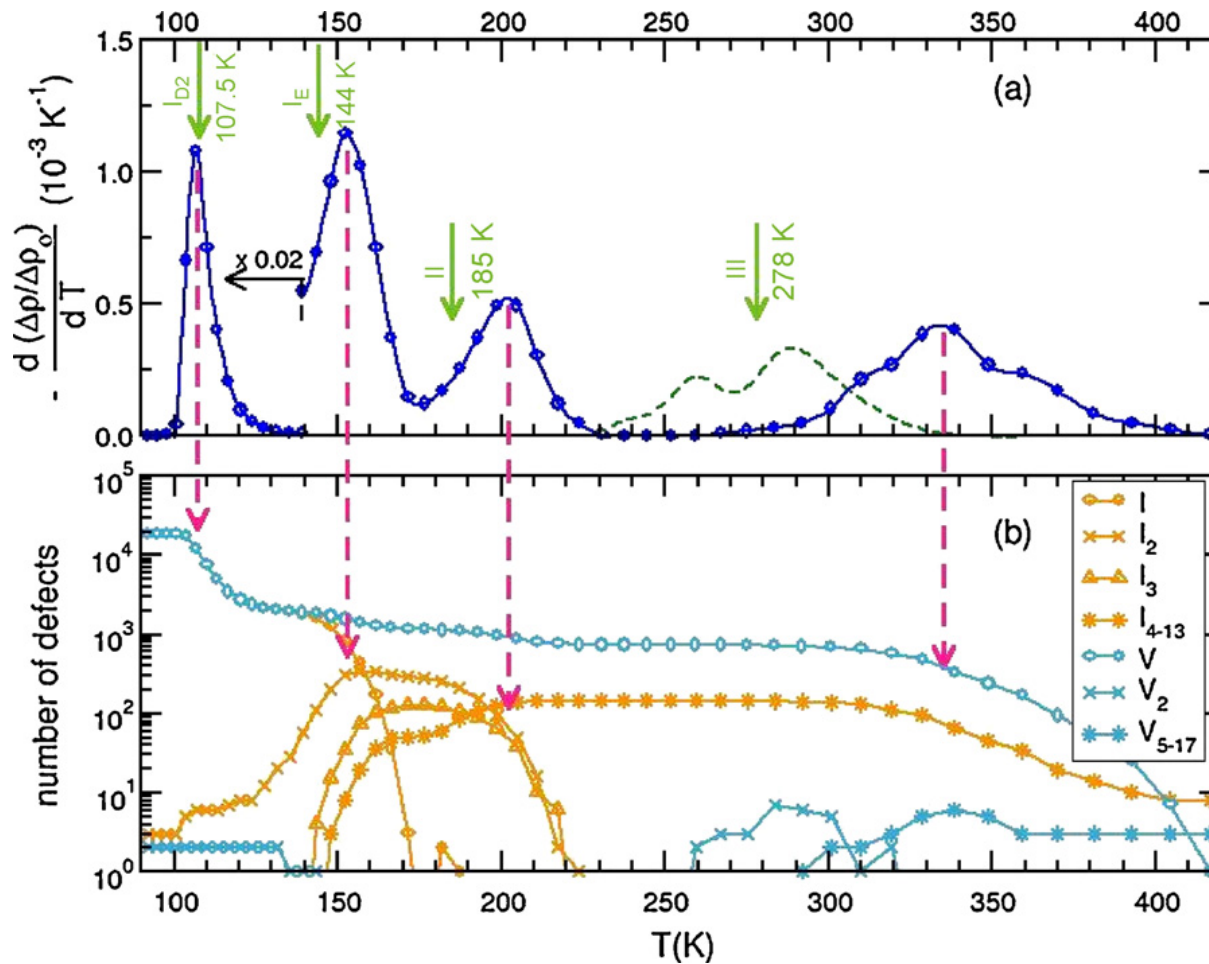
Recovery of electrical resistivity and defect population during isochronal annealing after electron irradiation:

a) temperature derivative of the simulated resistivity recovery stages. Green arrows indicate the positions of experimental peaks.

b) Associated defect population evolution for 16×109 atoms. The magenta dashed lines indicate the position of the peak in the simulation.

The Fe-Cr system

- FeCr is the base alloy of the 9-12% Cr ferritic/martensitic steels that are the main candidates for structural components of fusion and Gen IV fission reactors

In Fe Cr alloys, antiferromagnetic Cr is added to a matrix of ferromagnetic Fe. This defines the thermodynamic behavior of the alloy: there is a tendency to short range order for low Cr and to clustering for higher Cr contents, resulting in an anomaly of the heat of formation
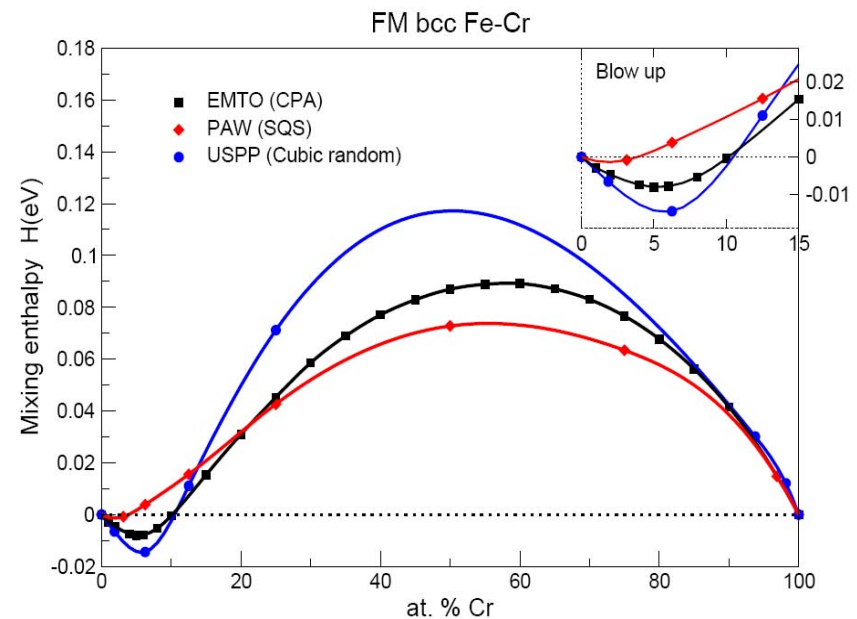
The case of Fe-Cr alloys

A number of measurements have been performed for dilute alloys (Maury (1987), Benkaddour (1987) Nikolaev (1997, 1999), Abe (1999)

The features associated with the annealing of RR of concentrated alloys in stage I can be explained by the formation, migration and trapping of mixed Fe-Cr dumbbells at a second Cr atom

Irradiation that produces small cascades stimulates the formation of mobile di-interstitials probably formed at the cascade quenching
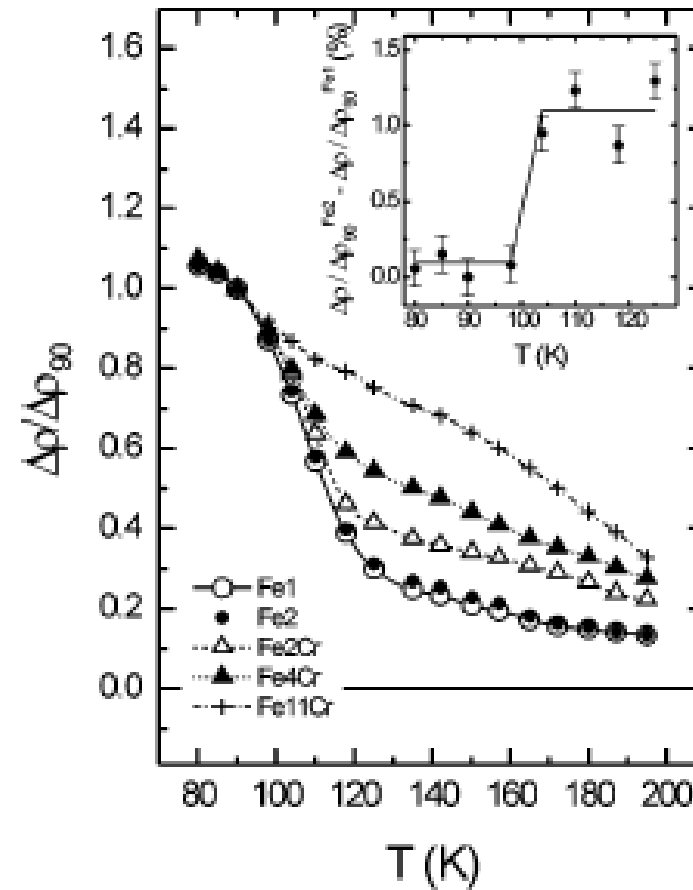
Defect accumulation in FeCr

- The mobile [111] cluster that will result from the [110] clustering have a high mobility and are expected to rapidly move out from the (thin) sample observed in TEM. But as indicated in the talks of Malerba and Samaras the clusters are pinned by the presence of Cr. It is therefore interesting to see their behaviour after irradiation of alloys with increasing Cr concentration.

- Irradiation experiments have been performed in a series of FeCr alloys with increasing Cr content

Experimental methodology

- Materials:
  - Alloys prepared from 99,99 Fe and Cr by arc melting in a pure Ar atmosphere. Nominal concentrations: 1, **2**, 3, **5**, 7, 10, **12** y 15% at Cr.
  - Effect of Cr content

- Ion irradiation conditions
  - Irradiations performed in the AIM facility of the Forschungszentrum Dresden-Rossendorf (FZD)*:
    - Fe^+ 150 keV
    - Dose: $2x10^{18}$ ions/m² (~0.8 dpa)
    - Flux: $2x10^{15}$ ions/m² s
    - Temperatures: 140K and 300K

- TEM observation at RT
  - JEOL 200 keV

Irradiation Temperature

300 K

140 K

Irradiation time

Observation time
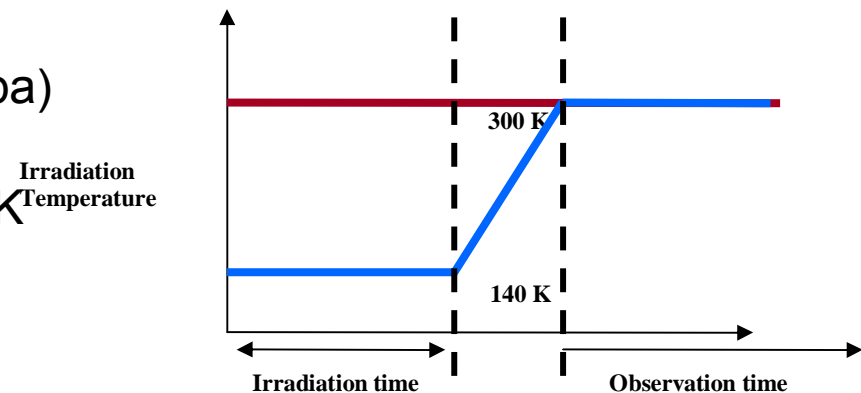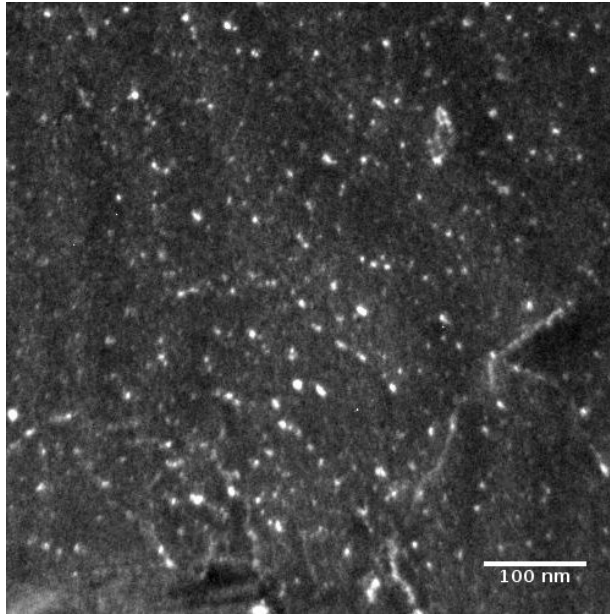
Fe12Cr 300K
g=200
1/3 of <100> are visible
All the <111> are visible

Fe12Cr 300K g=0-11
2/3 of <100> are visible
½ of <111> are visible

Fe12Cr 300K g=10-1
2/3 of <100> are visible
½ of <111> are visible
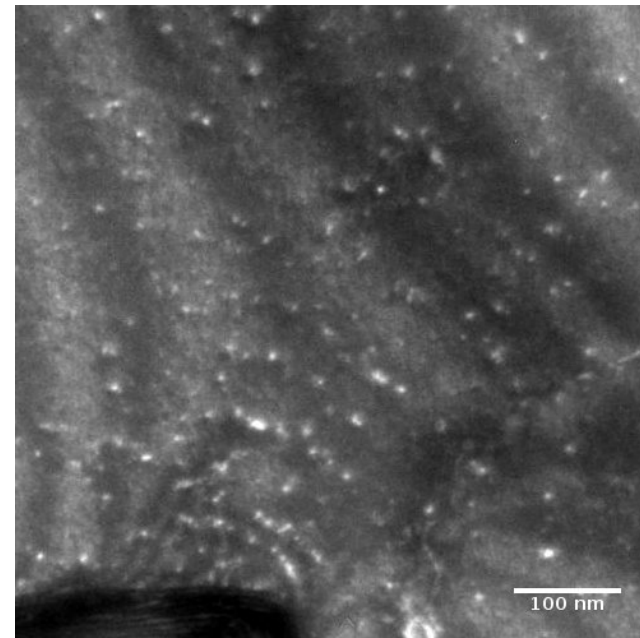
density of loops
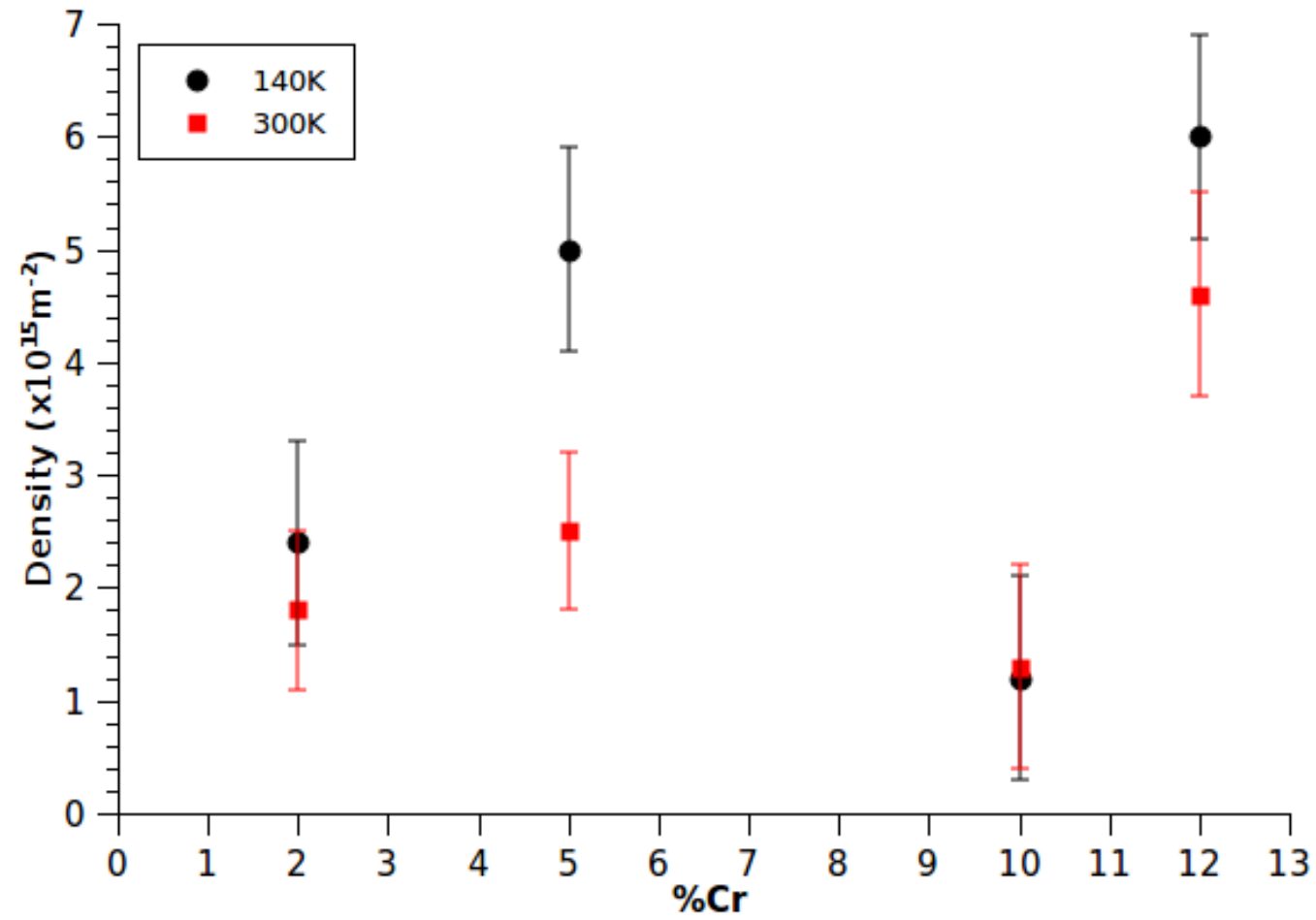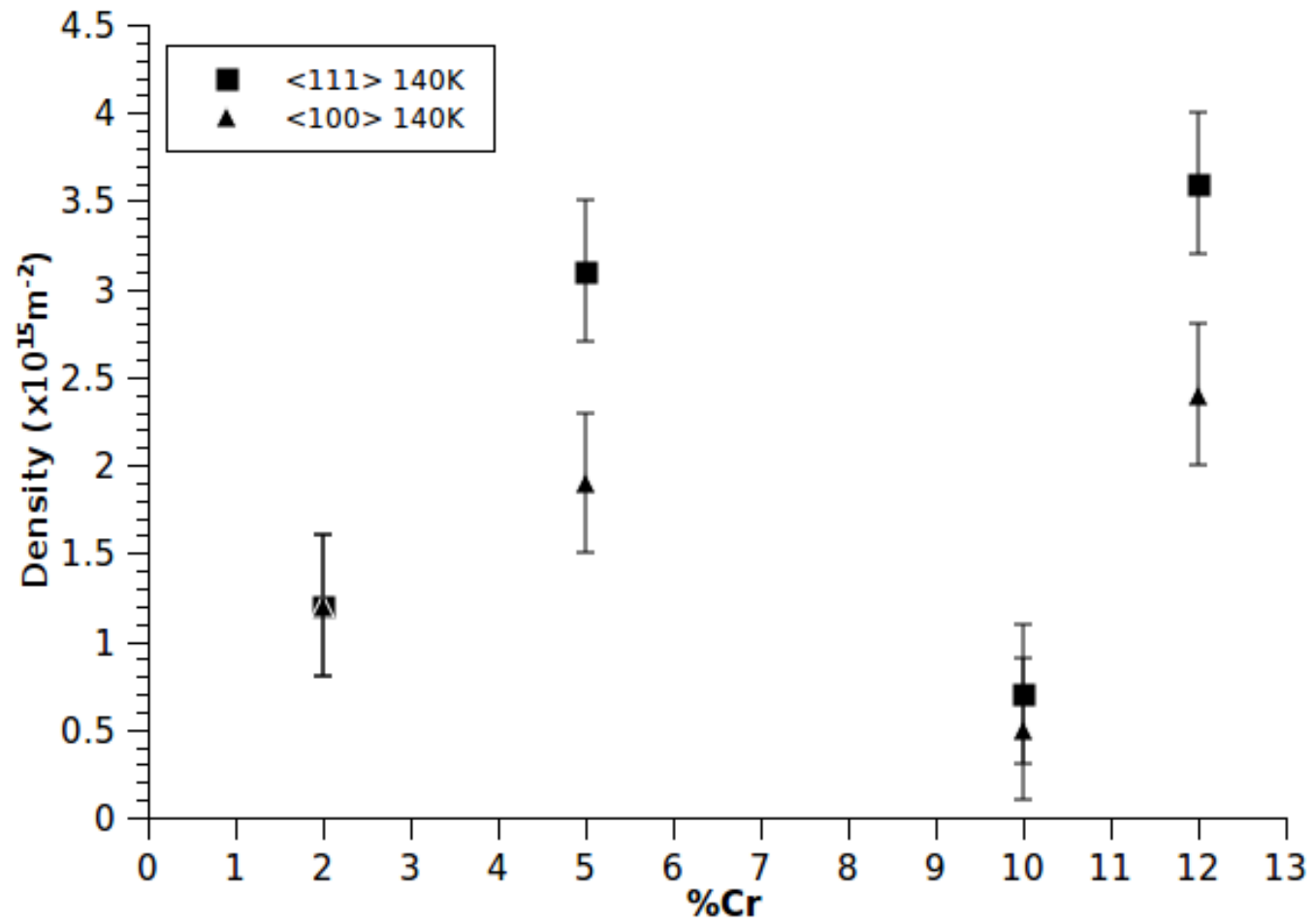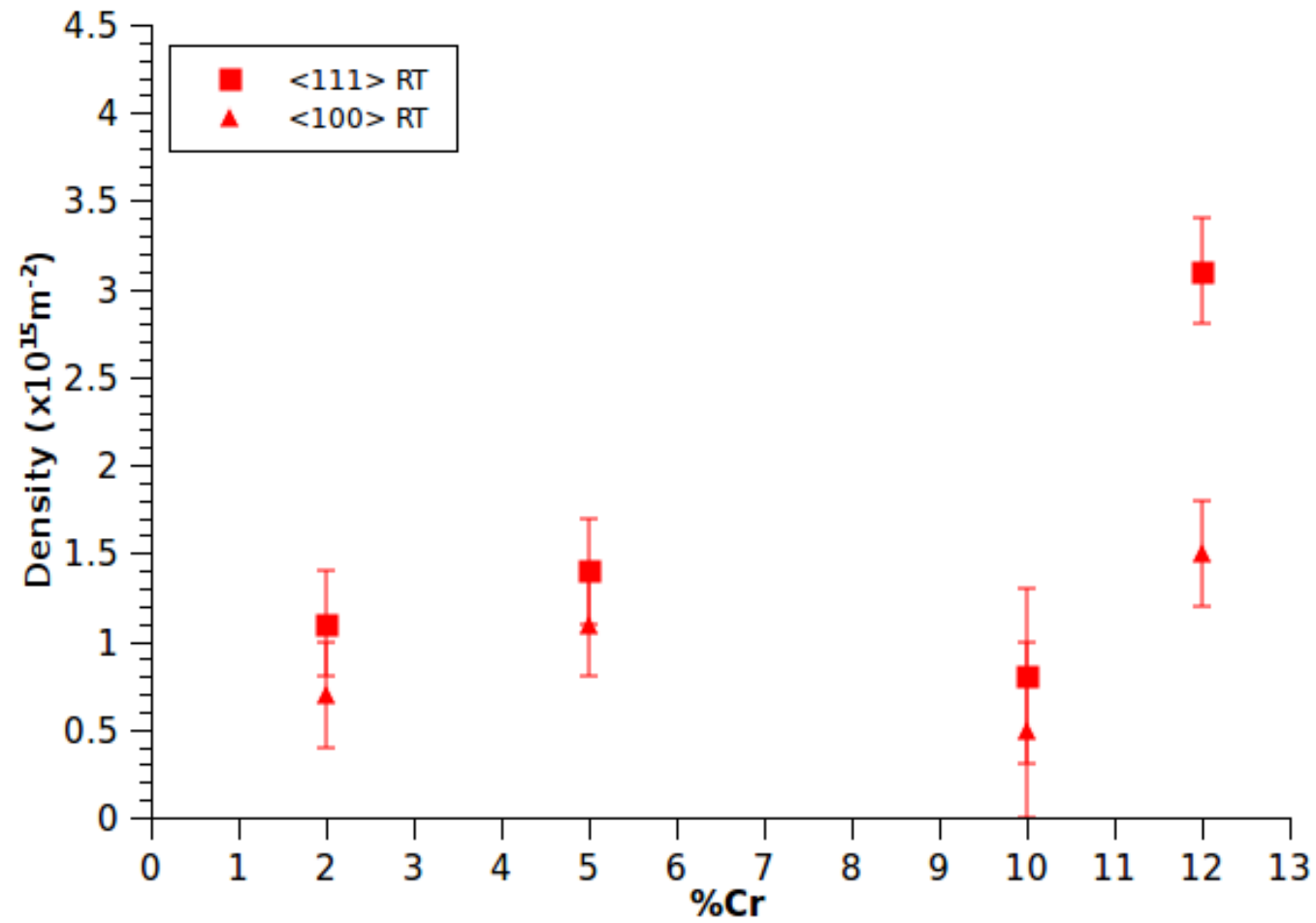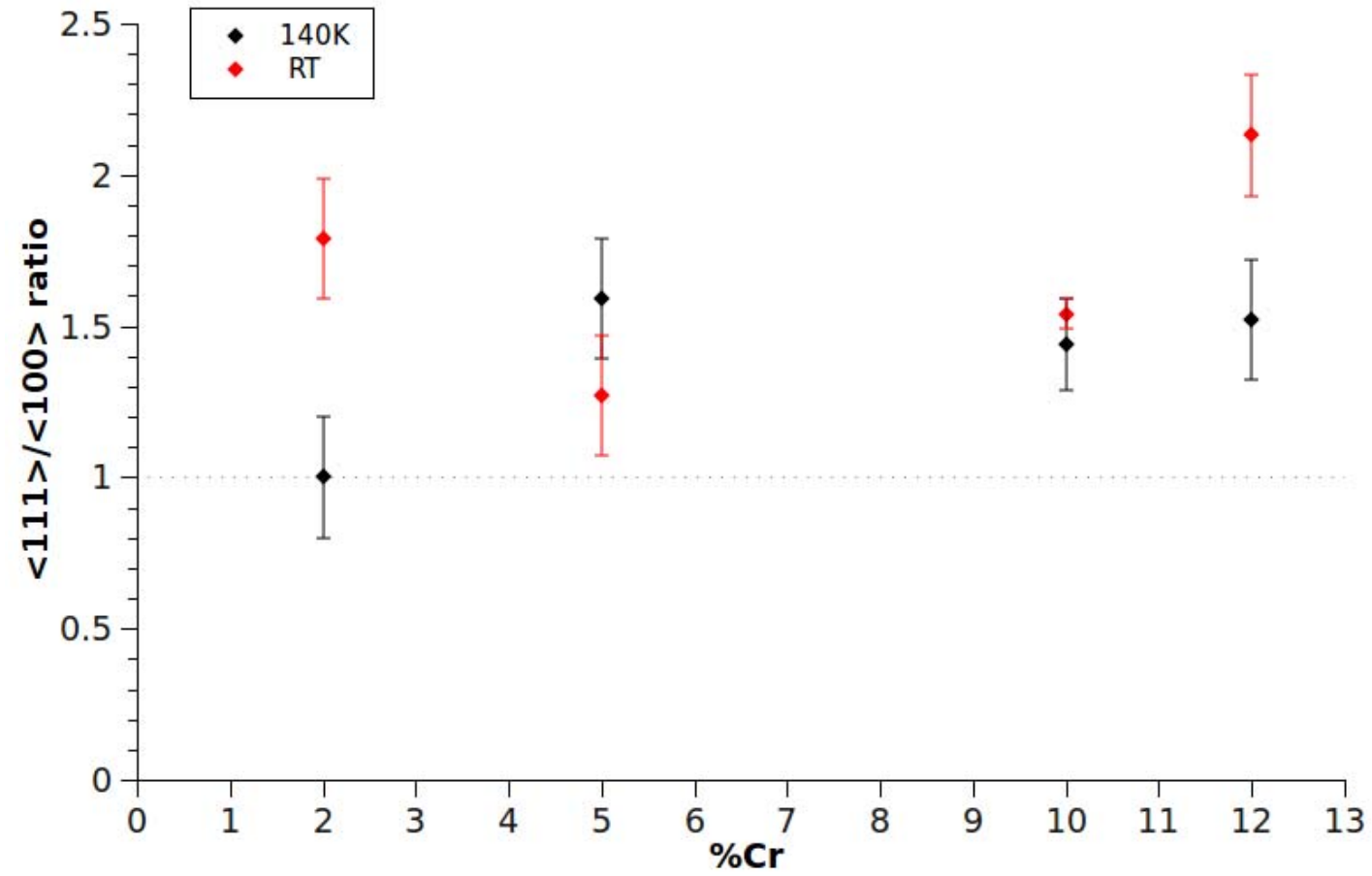
Effect on size distribution

T irr: 140 K

2.15 ± 0.06 nm	2.00 ± 0.06 nm	2.08 ± 0.07 nm	1.95 ± 0.07 nm

T irr: 300 K

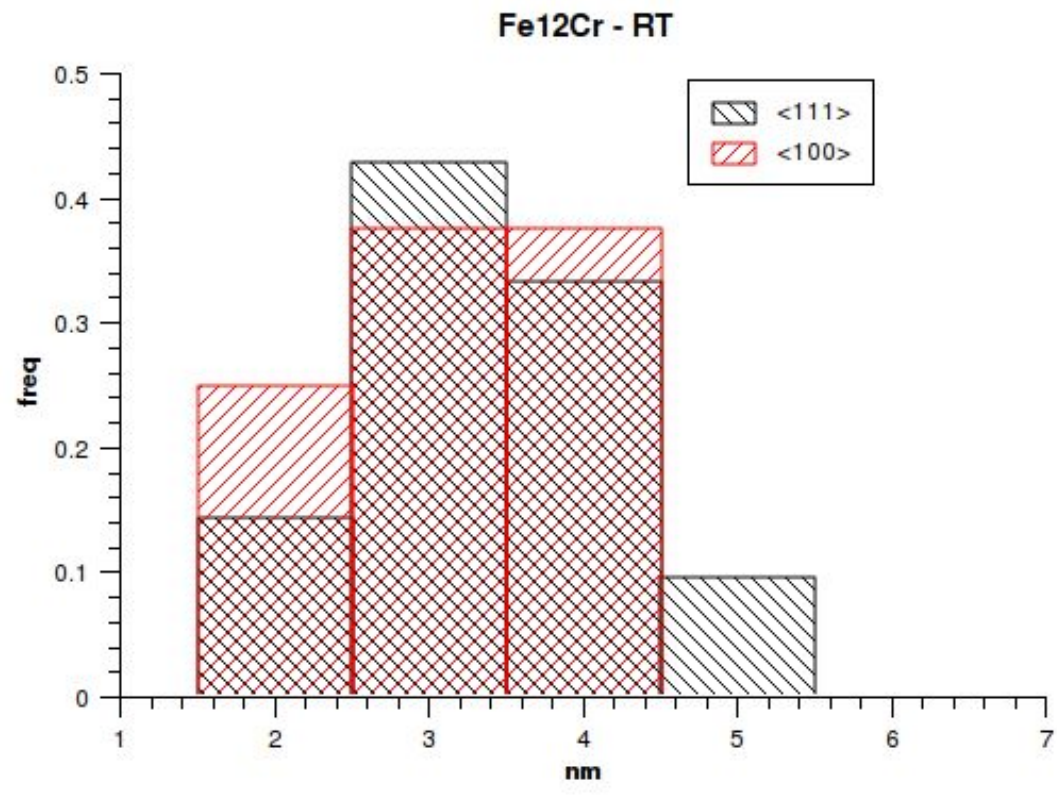|			
1.99 ± 0.05 nm	2.12 ± 0.08 nm	2.15 ± 0.02 nm	1.92 ± 0.15 nm
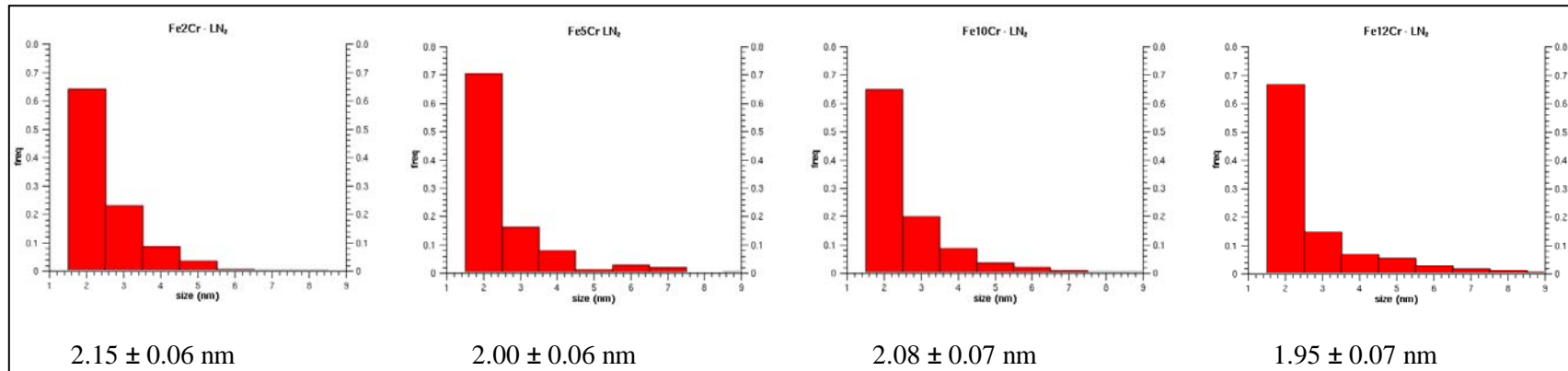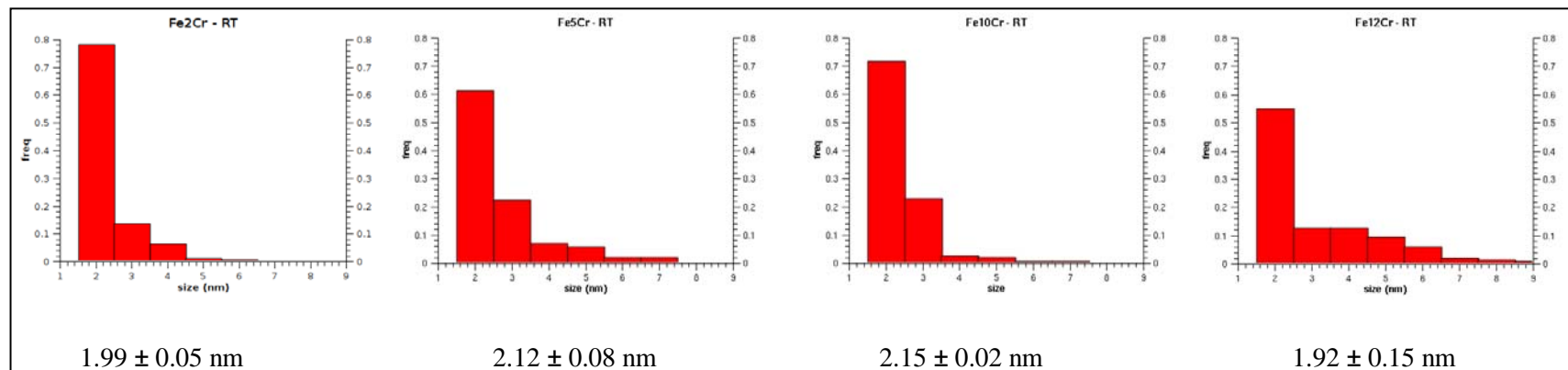
- No effect on average size is observed for different Cr content or irradiation temperature

- Maximum size seems to increase for higher Cr content

The question that arises from these results is the presence of sesile [100] loops. They had been observed previously in Fe and steels
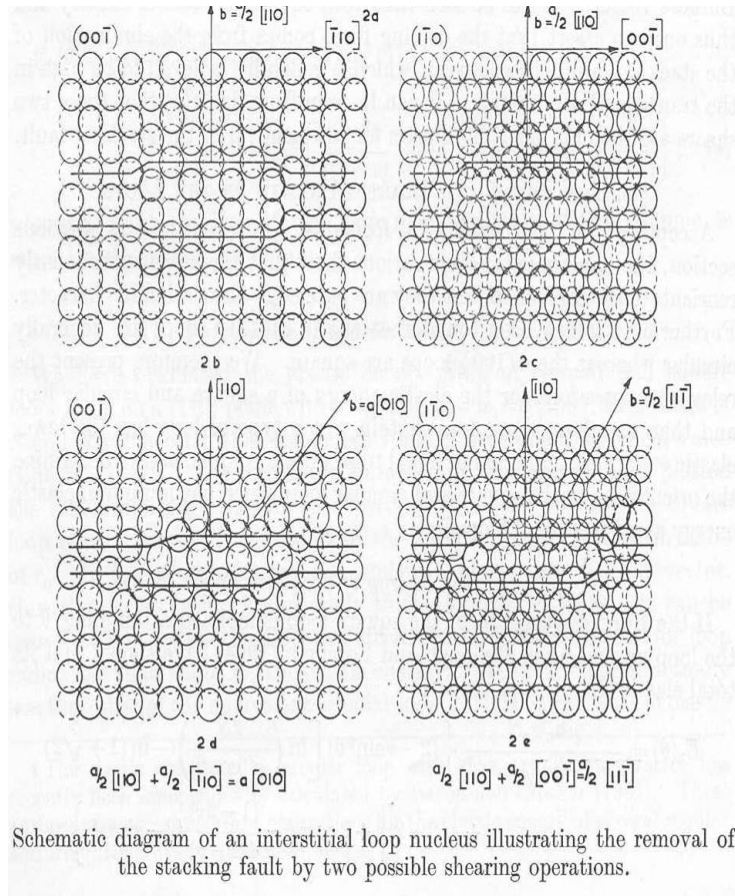
But their behavior in the present set of results is difficult to understand.

Two models have been proposed to explain the formation from 1/2 [111] loops, but none of the two would explain the presence of these loops at low irradiation temperatures (140 K)

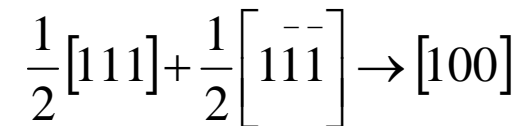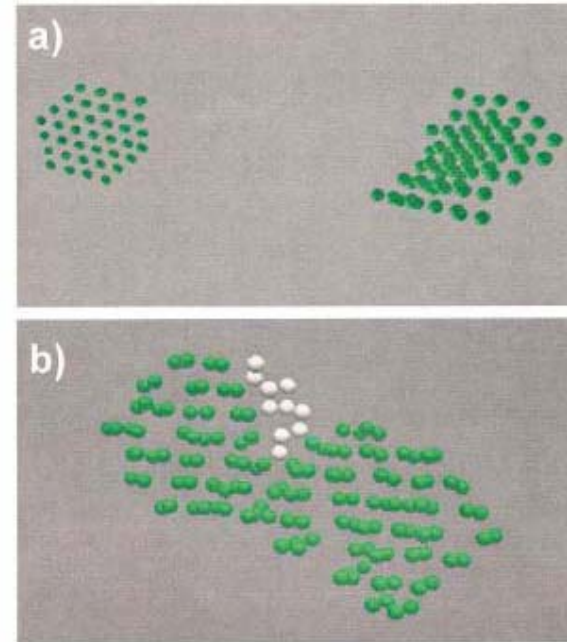It is though at present that the [100] Loops originate from the evolution of the cascade itself

Mechanism of formation of (100) loops

Shear of <110> loops

Interaction between <111> loops

Schematic diagram of an interstitial loop nucleus illustrating the removal of the stacking fault by two possible shearing operations.

Eyre & Bullough (1965)

$$\frac{1}{2}\left[111\right]+\frac{1}{2}\left[1\bar{1}\bar{1}\right]\rightarrow\left[100\right]$$

Marian et al (2002)